



Acoustic Array Interaction In the Time Domain

Dr. George W Benthien

May 5, 2008

E-mail: george@gbenthien.net

Contents

1	Introduction	2
2	Acoustic Impulse Functions	4
3	Some Notes on Numerical Fourier Transforms	11
4	Transducer Element and Array Description	13
5	Calculation of the Impulse Response Functions for the Array	16
6	The Array Solution Procedure	18
7	Computed Results for Some Transducer Arrays	25
8	Summary	37
	References	38

1 Introduction

The acoustic interactions in transducer arrays have typically been analyzed in the frequency domain. There have been a number of techniques developed for this purpose. However, when dealing with nonlinear transducers or if the transient behavior is of interest, it is more convenient to work in the time domain. In this paper a method will be presented for analyzing acoustic array interactions in the time domain. This method will be applied to a simple transducer array.

In the frequency domain array interactions are usually expressed in terms of mutual radiation impedances. For an array of one degree of freedom devices, the radiation force F_m^{rad} on the m -th element is expressed as

$$F_m^{\text{rad}}(\omega) = \sum_{n=1}^N z_{mn}(\omega)v_n(\omega) \quad (1)$$

where z_{mn} is the mutual radiation impedance between the m -th and n -th elements, v_n is the velocity of the n -th element, and ω is the angular frequency. For multimode devices, an equation like (1) can be written, but in this case F_m^{rad} and v_n are vectors of modal coefficients and each z_{mn} is a square matrix whose row and column dimensions are the number of modes used. The radiation force is expressed in terms of velocities since many of the equivalent circuits used to represent transducers employ velocities as currents and forces as voltages. However, for our purposes, it will be more convenient to use accelerations instead of velocities. In the frequency domain a velocity v is related to the corresponding acceleration a by $a = i\omega v$. Thus, equation (1) can be written in the form

$$F_m^{\text{rad}}(\omega) = \sum_{n=1}^N m_{mn}(\omega)a_n(\omega) \quad (2)$$

where $m_{mn} = z_{mn}/i\omega$. The coefficients m_{mn} are complex and have the units of mass. Taking the inverse Fourier transform of equation (2), we get

$$F_m^{\text{rad}}(t) = \sum_{n=1}^N \int_0^t \mu_{mn}(\tau)a_n(t - \tau) d\tau \quad (3)$$

where $F_m^{\text{rad}}(t)$ is the inverse transform of $F_m^{\text{rad}}(\omega)$, $a_n(t)$ is the inverse transform of $a_n(\omega)$, and $\mu_{mn}(t)$ is the inverse transform of $m_{mn}(\omega)$. Here, we have assumed that the radiation force and the accelerations are zero for times less than zero. We have also used the causality condition that $F_m^{\text{rad}}(t)$ can't depend on acceleration values corresponding to times greater

than t . The coefficient $\mu_{mn}(t)$ is the radiation force on the m -th element due to a unit acceleration impulse on the n -th element with all the other elements held rigid.

There are three main reasons for preferring accelerations over velocities. First, the acoustic pressure is more directly related to accelerations than it is to velocities. To produce an acoustic pressure it is necessary to compress the fluid. Since fluids such as water would rather flow than compress, compression is obtained by accelerating the radiating face of the element so that the inertia of the fluid opposes the flow. Second, the time-domain approach employed in this paper involves taking inverse Fourier transforms of either the z_{mn} or the m_{mn} to obtain the mutual impulse response functions. The inverse Fourier transform of the self radiation impedance z_{nn} doesn't exist in the ordinary sense, since the real part of z_{nn} doesn't approach zero as frequency increases. While this can be handled using delta functions, it introduces an unnecessary complication. Third, using accelerations leads to a more stable solution procedure. The self acceleration impulse response μ_{nn} is primarily a positive pulse similar to a smoothed delta function whereas the corresponding velocity impulse response has closely spaced positive and negative peaks similar to a smoothed derivative of a delta function. This alternation in sign leads to significant cancellation when the velocity impulse response is convolved with a smoothly varying velocity.

2 Acoustic Impulse Functions

I first considered using the Kirchhoff integral equation method for generating the functions $\mu_{mn}(t)$ directly in the time domain. I have used this method to successfully calculate the response for various acceleration pulses [1], but I haven't been able to get good accuracy for the very short pulses that are needed to approximate an impulse. Therefore, I decided to generate the functions $m_{mn}(\omega)$ in the frequency domain using the boundary element program CHIEF [2] and perform the inverse Fourier transform numerically to obtain $\mu_{mn}(t)$. Some care is necessary, especially for the self terms, since the convergence in the frequency domain is very slow. The imaginary part of $m_{mm}(\omega)$ only converges to zero like $1/\omega$ as $\omega \rightarrow \infty$.

Figure 1 shows the impulse response of a uniformly excited sphere

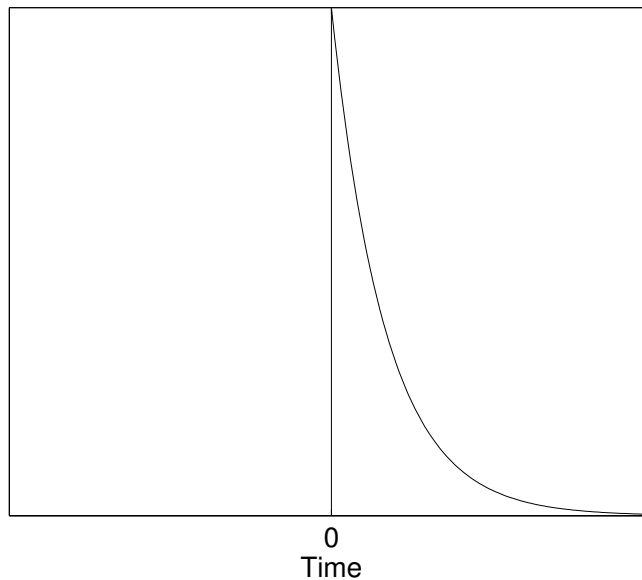


Figure 1: Radiation impulse response of a uniform sphere

Notice that the response is zero for negative times; it jumps to a finite value at $t = 0$; and then it decays to zero for large time. These are characteristics of all self radiation impulse responses. However, in many cases the self radiation impulse response oscillates as it approaches zero. The discontinuity at $t = 0$ is what gives rise to the slow convergence in the frequency domain. Typically, a function with jump discontinuities gives rise to $1/\omega$ convergence in the frequency domain; a function that is continuous gives rise to $1/\omega^2$ convergence; a continuous function with continuous first derivative gives rise to $1/\omega^3$ convergence, and so on. If the response is only defined over a finite interval (as it always is in numerical problems), then it is necessary to look at the smoothness of the periodic extension to determine the rate of convergence. In this case the discontinuities often occur at the end points.

We will now show how to modify the self impulse response so that it converges faster. Let $f(t)$ denote the self impulse response. Consider now the function $\hat{f}(t)$ defined by

$$\hat{f}(t) = \begin{cases} f(t) & \text{for } t \geq 0 \\ f(-t) & \text{for } t < 0. \end{cases} \quad (4)$$

This function reflects the positive time portion of f about the y-axis as shown in figure 2.

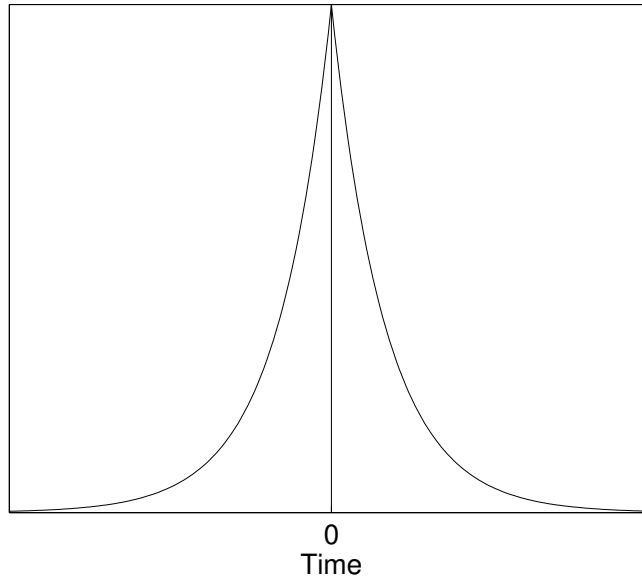


Figure 2: Spherical impulse with reflection

Notice that \hat{f} is continuous at $t = 0$. If $F(\omega)$ is the Fourier transform of f and $\hat{F}(\omega)$ is the Fourier transform of \hat{f} , then

$$\begin{aligned} \hat{F}(\omega) &= \int_{-\infty}^{\infty} \hat{f}(t) e^{-i\omega t} dt \\ &= \int_{-\infty}^0 f(-t) e^{-i\omega t} dt + \int_0^{\infty} f(t) e^{-i\omega t} dt \\ &= \int_0^{\infty} f(t) e^{i\omega t} dt + \int_0^{\infty} f(t) e^{-i\omega t} dt \\ &= F^*(\omega) + F(\omega) = 2\text{Real } F(\omega). \end{aligned} \quad (5)$$

Since $\text{Real } F(\omega)$ converges like $1/\omega^2$, we will get better results if we obtain $f(t)$ by inverse transforming $2\text{Real } F(\omega)$ and throwing away the half corresponding to negative times.

We will now show how to obtain $1/\omega^3$ convergence. It turns out that, for small times, the acoustic pressure p is approximately related to the normal velocity v by the plane wave relation $p = \rho c v$ where ρ is the fluid density and c is the sound speed. If the acceleration is an impulse, then the velocity will be a unit step function at $t = 0$. Thus, the pressure jumps from zero to ρc at $t = 0$. In computing the self radiation impulse response we are usually interested in some kind of radiation force. For a piston radiator the force would jump from zero to $\rho c A$ where A is the area of the piston. In other problems we are often interested in forces that are the integral of pressure times some shape function over the radiating area. In these problems A would be replaced by an effective area obtained by integrating the shape function over the area. In any case it is usually possible to obtain the value of the self radiation impulse response at $t = 0$. Consider the case of a piston radiator. If f is the impulse response, consider the modified function f_{mod} defined by

$$f_{\text{mod}}(t) = \begin{cases} f(t) - \rho c A e^{-\alpha t} & t \geq 0 \\ 0 & t < 0 \end{cases} \quad (6)$$

for some $\alpha > 0$. The function f_{mod} will be zero at $t = 0$ and will be approximately zero for large positive times. We will now extend the positive time portion of f_{mod} to negative times as an odd function, i.e., we define \hat{f}_{mod} by

$$\hat{f}_{\text{mod}}(t) = \begin{cases} f_{\text{mod}}(t) & \text{for } t \geq 0 \\ -f_{\text{mod}}(-t) & \text{for } t < 0. \end{cases} \quad (7)$$

Since f_{mod} vanishes at $t = 0$, the function \hat{f}_{mod} will be continuous and have a continuous first derivative. Thus, the Fourier transform of \hat{f}_{mod} will converge like $1/\omega^3$. It is easily verified that the transform of \hat{f}_{mod} is given by

$$\hat{F}_{\text{mod}}(\omega) = 2i \text{Imag } F_{\text{mod}}(\omega). \quad (8)$$

The transform of the function that is $\rho c A e^{-\alpha t}$ for positive t and zero for negative t is given by

$$\frac{\rho c A}{\alpha + i\omega} = \frac{\rho c A \alpha}{\alpha^2 + \omega^2} - i \frac{\rho c A \omega}{\alpha^2 + \omega^2}.$$

Therefore,

$$\text{Imag } F_{\text{mod}}(\omega) = \text{Imag } F(\omega) + \frac{\rho c A \omega}{\alpha^2 + \omega^2} \quad (9)$$

and hence

$$\hat{F}_{\text{mod}}(\omega) = 2i \left[\text{Imag } F(\omega) + \frac{\rho c A \omega}{\alpha^2 + \omega^2} \right]. \quad (10)$$

Thus, given $F(\omega)$, we can obtain $f(t)$ as follows:

1. Calculate $\hat{F}_{\text{mod}}(\omega)$ using equation (10).
2. Perform a numerical inverse Fourier transform of $\hat{F}_{\text{mod}}(\omega)$ to obtain $\hat{f}_{\text{mod}}(t)$.
3. For $t \geq 0$ compute $f(t)$ using $f(t) = \hat{f}_{\text{mod}}(t) + \rho c A e^{-\alpha t}$.

I have found that this technique gives very good self radiation impulse response functions. The choice of α is not very critical, but we want it to be large enough so that $e^{-\alpha t}$ is negligible when $f(t)$ is negligible and small enough so that it can be modeled using a reasonable time step. Thus, we would like the decay of $e^{-\alpha t}$ to be similar to that of $f(t)$. For the examples considered in this paper we used $\alpha = 2\pi/t_0$ where t_0 is three times the time required for sound to cross the piston.

The mutual impulse response functions don't have the same convergence problem. They vanish for $t = 0$ and are small for large times. They are also very smooth functions. Because of the fast convergence rate of their transforms, they can be computed directly by numerically performing an inverse Fourier transform of the frequency response. However, the mutual impulse response is zero for a period of time starting at zero and extending to the time required for sound to travel the minimum distance between the two elements. To avoid having to compute the response during this initial period, we shift the response to the left by applying an exponential multiplier to the frequency data. If d is the minimum separation between the two elements, then we multiply the frequency data by $e^{i\omega d/c}$. This causes the response in the time domain to be shifted to the left by d/c . To obtain the actual mutual impulse response, we insert zeroes in the initial period to shift the response back to the right.

As a test of this technique for calculating the self impulse response function, I apply it to a problem for which an analytical solution is available. Oscar Lindemann [4] derived an expression for the velocity impulse response $\zeta(t)$ of a square piston on an infinite plane rigid baffle. This response can be written as

$$\zeta(t) = \rho c [A\delta(t) - cf(ct)] \quad (11)$$

where $\delta(t)$ is the delta function and f is the function defined by

$$f(r) \begin{cases} 0 & r < 0 \\ 4\pi^{-1}(s - r/2) & 0 \leq r \leq s \\ 2\pi^{-1}[r - 2s(r^2 - s^2)^{1/2}/r] & s \leq r \leq s\sqrt{2} \\ 0 & s\sqrt{2} \leq r \leq \infty. \end{cases} \quad (12)$$

Here s is the length of a side of the square and $s\sqrt{2}$ is the maximum dimension of the square. A plot of the function $f(r)$ is shown in figure 3.

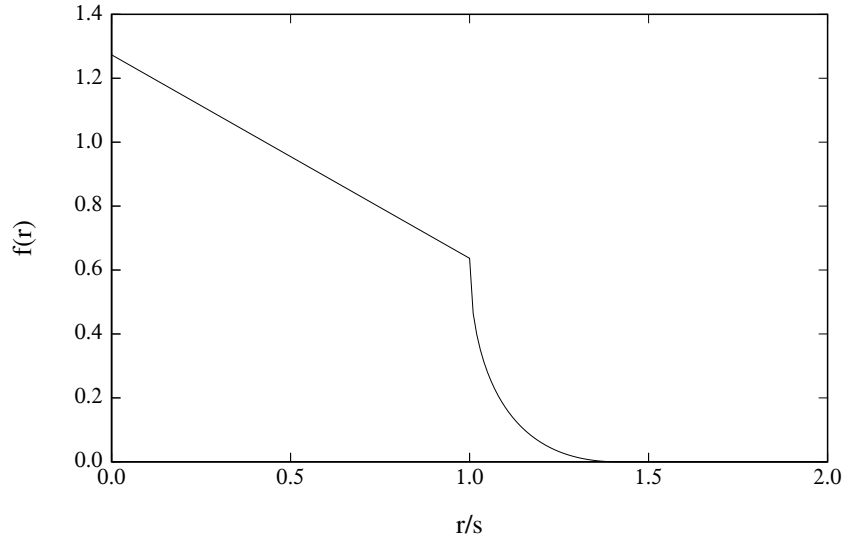


Figure 3: The function f used to calculate the impulse response of a square piston.

The expression for the acceleration impulse response $\mu(t)$ can be obtained by integrating equation (11), i.e.,

$$\mu(t) = \rho c A H(t) - \rho c^2 \int_0^t f(c\tau) d\tau = \rho c A H(t) - \rho c \int_0^{ct} f(r) dr. \quad (13)$$

In this equation $H(t)$ is the Heaviside step function that is zero for $t < 0$ and is one for $t \geq 0$. It turns out that f has the property

$$\int_0^{s\sqrt{2}} f(r) dr = A. \quad (14)$$

Therefore, $\mu(t)$ is identically zero for $t > s\sqrt{2}/c$.

To implement the numerical method described previously, the frequency response for the square piston was calculated using CHIEF [2] over the range $0 \leq s/\lambda \leq 3.3$ in steps of 0.3. Since the problem has two planes of symmetry, it was only necessary to subdivide one quarter of the piston. A 12×12 breakup of the quarter piston was used. The impulse response was obtained by performing an inverse Fast Fourier Transform of the modified frequency response defined as in equation (10) and then making the appropriate correction in the time domain. Figure 4 shows a comparison of the numerical result with the analytic result. The agreement is very good.

Figure 5 shows a similar comparison in which the numerical result was obtained by an inverse Fourier transform of the frequency response without the modifications described above. Here the agreement is not nearly as good. Thus, the modifications do improve the accuracy of the computed self impulse response, especially for small times.

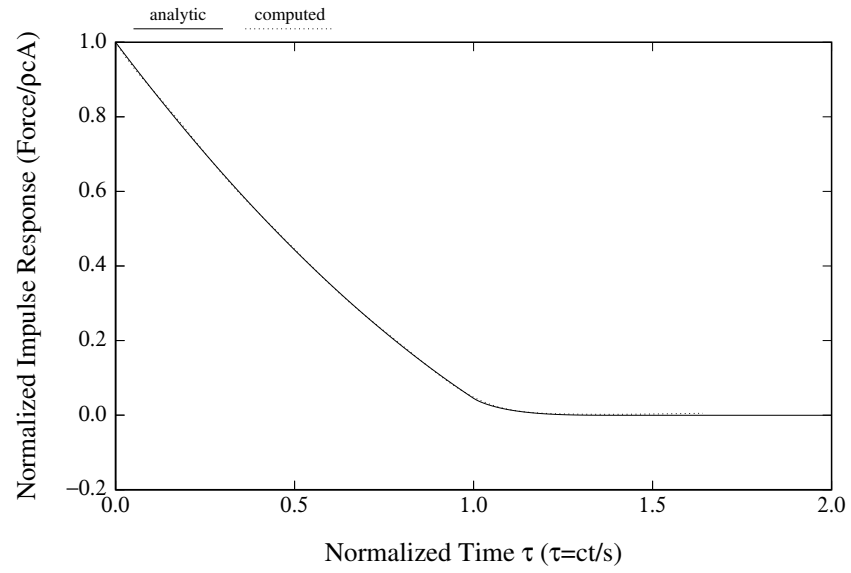


Figure 4: Analytic vs. numerical comparison using modified impulse response.

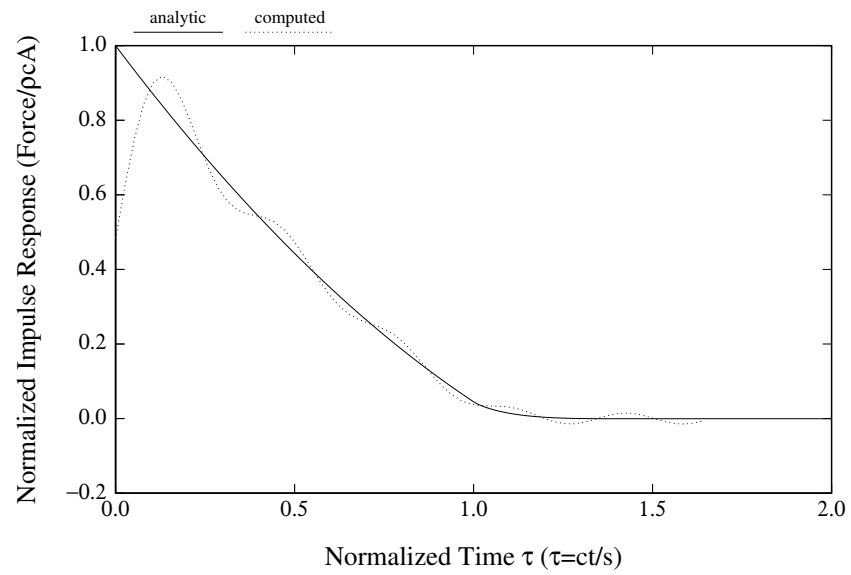


Figure 5: Analytic vs. numerical comparison without modifications.

3 Some Notes on Numerical Fourier Transforms

To compute impulse responses we would like to be able to calculate continuous Fourier transforms (Fourier Integrals). However, since we are limited to a finite number of function values, we must be satisfied with discrete Fourier transforms. These are usually packaged as Fast Fourier Transforms (FFTs). In this section we will review some of the relationships that exist between continuous and discrete Fourier transforms. Suppose $x(t)$ and $X(f)$ are a Fourier transform pair, i.e.,

$$x(t) = \int_{-\infty}^{\infty} X(f)e^{i2\pi ft} df \quad (15a)$$

$$X(f) = \int_{-\infty}^{\infty} x(t)e^{-i2\pi ft} dt. \quad (15b)$$

Let Δt be the time increment and let $T = N\Delta t$ where N is the number of equally spaced sampled values. Let $\Delta f = 1/T$ be the frequency increment and define F by $F = N\Delta f = 1/\Delta t$. Consider the functions

$$x_p(t) = \sum_{k=-\infty}^{\infty} x(t + kT) \quad (16a)$$

$$X_p(f) = \sum_{k=-\infty}^{\infty} X(f + kF). \quad (16b)$$

The function x_p is periodic with period T and X_p is periodic with period F . Moreover x_p and X_p satisfy

$$x_p(m\Delta t) = \frac{1}{N} \sum_{n=0}^{N-1} FX_p(n\Delta f)e^{i2\pi mn/N} \quad (17a)$$

$$FX_p(n\Delta f) = \sum_{m=0}^{N-1} x_p(m\Delta t)e^{-i2\pi mn/N}, \quad (17b)$$

i.e., $\{x_p(m\Delta t)\}$ and $\{FX_p(n\Delta f)\}$ are a discrete Fourier transform pair. We will now show that, under certain conditions, X_p is a good approximation to X and x_p is a good approx-

imation to x . If $X(f)$ is negligible for $|f| \geq F/2$, then it follows from equation (16b) that

$$X_p(n\Delta f) \doteq X(n\Delta f) \quad 0 \leq n \leq N/2 \quad (18a)$$

$$X_p((N-n)\Delta f) \doteq X(-n\Delta f) \quad 0 \leq n \leq N/2. \quad (18b)$$

Similarly, if $x(t)$ is negligible for $|t| \geq T/2$, then it follows from equation (16a) that

$$x_p(m\Delta t) \doteq x(m\Delta t) \quad 0 \leq m \leq N/2 \quad (19a)$$

$$x_p((N-m)\Delta t) \doteq x(-m\Delta t) \quad 0 \leq m \leq N/2. \quad (19b)$$

Aliasing occurs when terms with $k \neq 0$ contribute significantly to the sum on the right-hand-side of equation (16a) or (16b). In order to prevent aliasing it is necessary for $X(f)$ to be negligible when $|f| \geq F/2$. Similarly, it is necessary for $x(t)$ to be negligible when $|t| \geq T/2$. Notice that the values for negative frequencies occur in reverse order in the last half of the sequence $\{X_p(n\Delta f)\}_{n=0}^{N-1}$. Similarly, the values for negative times occur in reverse order in the last half of the sequence $\{x_p(m\Delta t)\}_{m=0}^{N-1}$. If the function $x(t)$ is real-valued, then the negative frequency values are the complex conjugate of the corresponding positive frequency values. Notice also that the frequency values $X_p(n\Delta f)$ must be multiplied by F ($F = 1/\Delta t$) prior to performing the inverse discrete Fourier transform to get the time values $x_p(m\Delta t)$. We can get interpolated values in the time domain by padding the frequency sequence with a sequence of zeroes. These zeroes go in the middle—between the positive and negative frequency values—since this is where the large positive and negative frequency values reside. For best efficiency it is best to choose the number of sampled values N to be a power of two.

4 Transducer Element and Array Description

To illustrate the use of radiation impulses in array interaction problems we will consider a line array where each transducer is a simple device as pictured in figure 6.

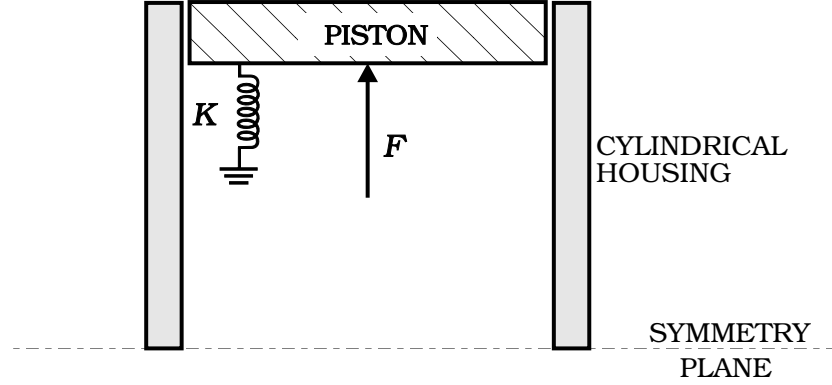


Figure 6: Simple linear transducer element.

It consists of two circular pistons each of mass M located at the ends of a rigid cylindrical housing. A spring of stiffness K restrains each piston and each piston is driven by a time varying force F . We will also assume that the pistons are viscously damped. The differential equation describing this transducer is given by

$$M\ddot{u} + R\dot{u} + Ku = F - F^{\text{rad}}. \quad (20)$$

Here u is the normal displacement of the piston, R is the damping resistance, and F^{rad} is the acoustic radiation force on the element. There is an equation like this for each element in the array. It follows from equations (3) and (20) that the following relations hold for the m -th element of the array:

$$Ma_m + Rv_m + Ku_m = F - \sum_{n=1}^N \int_0^t \mu_{mn}(\tau) a_n(t - \tau) d\tau \quad (21a)$$

$$\dot{v}_m = a_m \quad (21b)$$

$$\dot{u}_m = v_m. \quad (21c)$$

Finite element models of transducer elements lead to similar looking equations in which the scalar quantities M , K , R , and μ_{mn} become matrices and the quantities F , a_m , v_m , and u_m become vectors.

It will be convenient to introduce the dimensionless variables shown below in Table 1. Here $s = 2r$ is the diameter of each piston.

Table 1: Normalized variables.

$\bar{F}(\bar{t}) = \frac{1}{\rho s^2 c^2} F(s\bar{t}/c)$	drive force	$\bar{t} = \frac{t}{s/c}$	time
$\bar{u}(\bar{t}) = \frac{1}{s} u(s\bar{t}/c)$	displacement	$\bar{f} = s/\lambda$	frequency
$\bar{v}(\bar{t}) = \frac{1}{c} v(s\bar{t}/c)$	velocity	$\bar{M} = \frac{M}{\rho s^3}$	mass
$\bar{a}(\bar{t}) = \frac{s}{c^2} a(s\bar{t}/c)$	acceleration	$\bar{K} = \frac{K}{\rho c^2 s}$	stiffness
$\bar{\mu}(\bar{t}) = \frac{1}{\rho c s^2} \mu(s\bar{t}/c)$	interaction	$\bar{R} = \frac{R}{\rho c s^2}$	resistance

In terms of these dimensionless parameters, the equations in (21) become

$$\bar{M}\bar{a}_m + \bar{R}\bar{v}_m + \bar{K}\bar{u}_m = \bar{F}_m - \sum_{n=1}^N \int_0^{\bar{t}} \bar{\mu}_{mn}(\bar{\tau})\bar{a}_n(\bar{t} - \bar{\tau}) d\bar{\tau} \quad (22a)$$

$$\frac{d\bar{v}_m}{d\bar{t}} = \bar{a}_m \quad (22b)$$

$$\frac{d\bar{u}_m}{d\bar{t}} = \bar{v}_m \quad m = 1, \dots, N. \quad (22c)$$

Notice that the equations in (22) have the same form as the equations in (21). For the examples considered in this paper the height of the cylinder was taken to be equal to the radius of the piston. To make sure that the acoustic radiation affects the resonance, the mass M of the piston was taken to be equal to the low frequency radiation mass of the piston, i.e.,

$$M = M_{\text{rad}} = \frac{\rho s^3}{3}. \quad (23)$$

This results in $\bar{M} = 1/3$. Let f_m be the fluid-loaded resonant frequency of a single element and let λ_m be the corresponding wavelength. This resonant frequency is given approximately by

$$\omega_m^2 \doteq \frac{K}{M + M_{\text{rad}}} = \frac{K}{2M}. \quad (24)$$

Thus,

$$\bar{K} = \frac{K}{\rho c^2 s} \doteq \frac{2\omega_m^2 M}{\rho c^2 s} = \frac{2\omega_m^2 \rho s^3 \bar{M}}{\rho c^2 s} = \frac{8\pi^2}{3} \left(\frac{s}{\lambda_m} \right)^2. \quad (25)$$

In the examples of this paper we will specify s/λ_m and compute \bar{K} using equation (25). The viscous damping resistance R will be determined by specifying various values for the quality factor Q . Since $Q = \omega_m M/R$, it follows that $R = \omega_m M/Q$ and hence $\bar{R} = 2\pi(s/\lambda_m)\bar{M}/Q$.

In this paper we will consider two types of waveforms for the drive forces. One is a sinusoidal drive of the form

$$F_m(t) = |F|_m \sin \omega t \quad t \geq 0.$$

In terms of normalized coordinates this reduces to

$$\bar{F}_m(\bar{t}) = \frac{|F|_m}{\rho s^2 c^2} \sin\left(2\pi \frac{s}{\lambda} \bar{t}\right) \quad \bar{t} \geq 0.$$

To simplify matters we will set the normalized force amplitude $|F|_m/(\rho s^2 c^2)$ to one, i.e.,

$$\bar{F}_m(\bar{t}) = \sin\left(2\pi \frac{s}{\lambda} \bar{t}\right) \quad \bar{t} \geq 0. \quad (26)$$

The second type of waveform is a pulse consisting of one-half cycle of the waveform shown in equation (26). Since the normalized equations in (22) have the same form as the unnormalized equations in (21), we will drop the over bars in the rest of this paper and assume that all variables are normalized. Although the equations describing this device are linear, the technique described here can also be applied to nonlinear devices as long as the nonlinearity doesn't involve the highest order derivative, the acceleration a_m . For the array we will restrict ourselves to a line array as shown in figure 7. The number of elements will be variable.

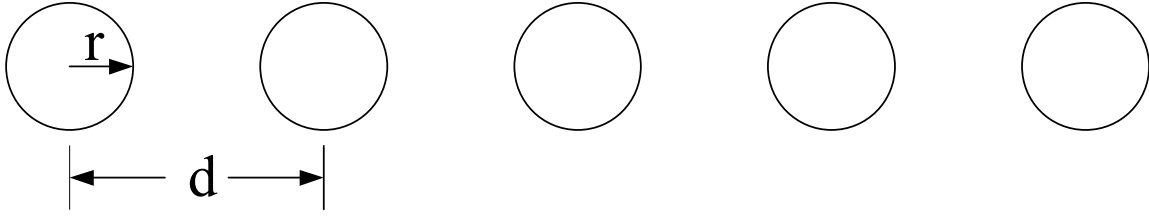


Figure 7: A line array shown here with five elements.

5 Calculation of the Impulse Response Functions for the Array

It was found for the examples considered in this paper that the self impulse response was virtually identical for all elements in the array and that there was virtually no effect due to the presence of the other elements (this may not be true for other problems). Therefore, the self impulse response was computed for a single element in the free-field using the axisymmetric boundary element program AXICHIEF [3]. Ten subdivisions were used along each piston radius and ten along the side for a total of 30. The frequency response due to a constant piston acceleration of one was computed over the range $0 \leq s/\lambda \leq 3.4$ in steps of 0.1. The impulse response in the time domain was computed using the method described previously having a convergence rate of $1/\omega^3$. The calculated self impulse response μ is shown in figure 8. To show the effect of increasing the convergence rate, figure 9 is a plot of the direct numerical inverse transform of the frequency data.

Figure 10 shows the mutual impulse function μ_{13} for a five element array with interelement spacing $d = 2s$. Notice that the response is zero at the beginning for the amount of time it takes for sound to travel the minimum distance between the two elements. The mutual impulse responses were calculated by numerically performing an inverse Fourier transform of the frequency data generated using the boundary element program CHIEF [2]. A time shift was employed as discussed previously. Zero padding was used to produce better resolution in the time domain. The line array was modeled using two planes of symmetry. Thus, we needed to subdivide one quarter of each element— half of the top piston and one quarter of the side. Half of each upper piston was modeled using 4 subdivisions in the radial direction and 12 subdivisions in the angular direction. One quarter of the side was modeled using 2 subdivisions in the axial direction and 12 subdivisions in the angular direction. Thus there were 72 subdivisions on each element and a total of 360 for the five element array. The frequency response was computed over the range $0 \leq s/\lambda \leq 2$ in steps of 0.1.

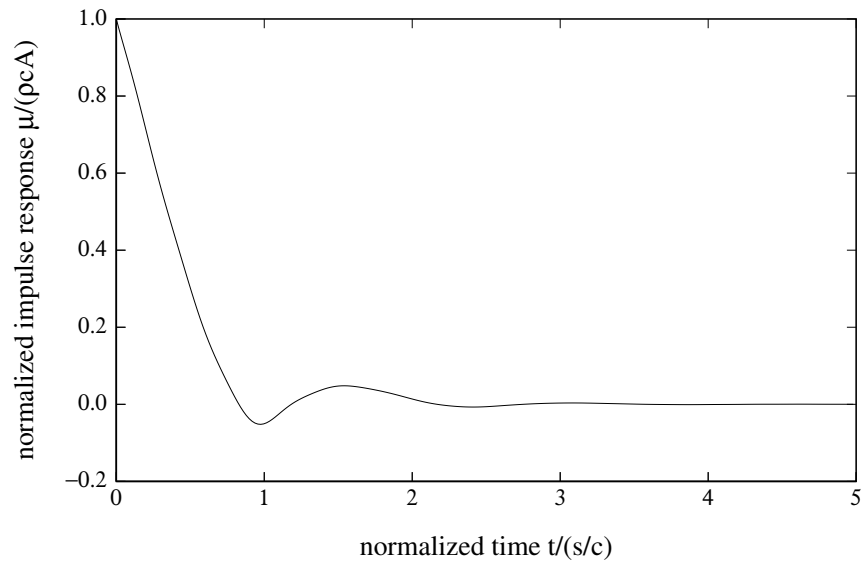


Figure 8: Normalized self impulse response.

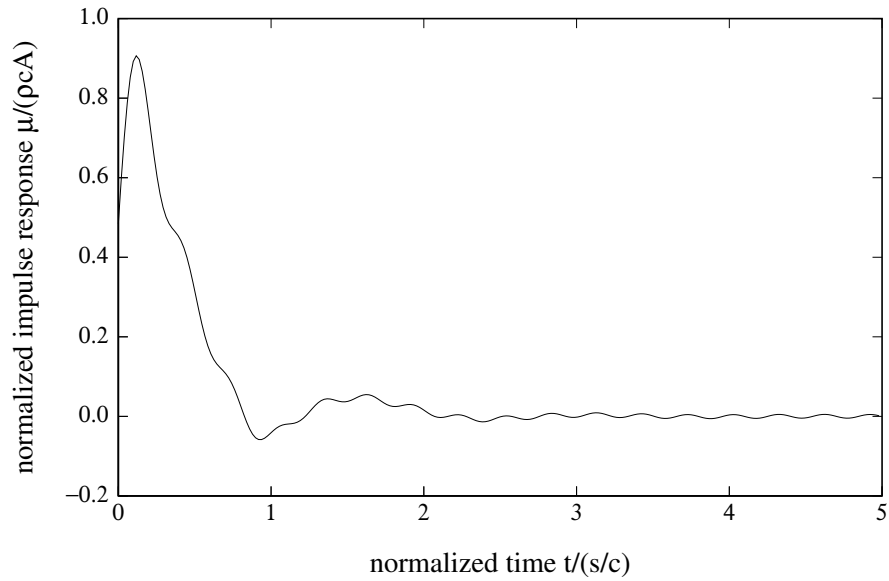


Figure 9: Uncorrected self impulse response.

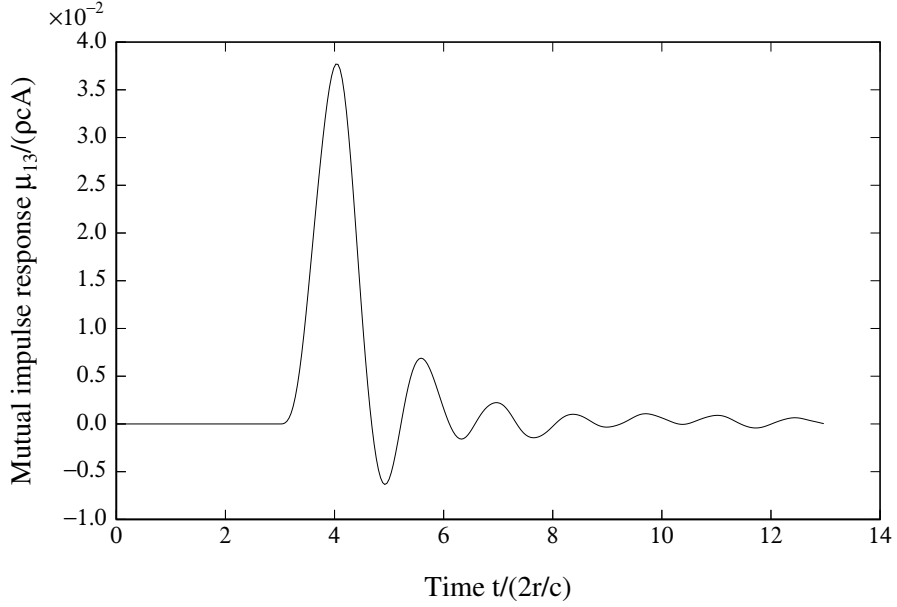


Figure 10: The mutual impulse response μ_{13} .

6 The Array Solution Procedure

The equations in (21) form a system of differential-integral equations. We will use a time stepping procedure for solving these equations that is similar to ones used in solving systems of ordinary differential equations. It should be noted that there is a delay before the force on the m -th element is affected by an acceleration of the n -th element, $m \neq n$. This delay is the time required for sound to travel the minimum separation between the elements. We will assume that the time step δ in our procedure is less than the time required for sound to travel the minimum separation between any two elements. This assumption is not strictly needed, but it does simplify the procedure by providing a partial decoupling of the element equations. Suppose we have calculated a_m , v_m , and u_m for time steps up through $t_r = r\delta$. We will show how to use standard differential equation solvers to advance the solution to the next time step. Let t lie in the next time interval $[t_r, t_{r+1}]$.

The impulse response integrals on the right-hand-side of equation (21a) can be split as follows

$$\int_0^t \mu_{mn}(\tau) a_n(t - \tau) d\tau = \underbrace{\int_0^{t-t_r} \mu_{mn}(\tau) a_n(t - \tau) d\tau}_{a_n \text{ in current interval}} + \underbrace{\int_{t-t_r}^t \mu_{mn}(\tau) a_n(t - \tau) d\tau}_{a_n \text{ in past history}}. \quad (27)$$

Because of our assumption on the step size, we have $\mu_{mn}(\tau) = 0$ for $\tau \leq \delta$ when $m \neq n$.

Since $t - t_r \leq \delta$, we have

$$\int_0^{t-t_r} \mu_{mn}(\tau) a_n(t - \tau) d\tau = 0 \quad m \neq n. \quad (28)$$

Since μ_{mm} typically varies faster than a_m , the corresponding integral for $m = n$ will be calculated by assuming that a_m varies linearly over the interval $[0, t - t_r]$, i.e.,

$$a_m(t - \tau) \doteq \frac{a_m(t_r) - a_m(t)}{t - t_r} \tau + a_m(t) \quad 0 \leq \tau \leq t - t_r. \quad (29)$$

Using this relation, it follows that

$$\begin{aligned} \int_0^{t-t_r} \mu_{mm}(\tau) a_m(t - \tau) d\tau &\doteq a_m(t) \left[\int_0^{t-t_r} \mu_{mm}(\tau) d\tau - \frac{1}{t - t_r} \int_0^{t-t_r} \tau \mu_{mm}(\tau) d\tau \right] \\ &\quad + a_m(t_r) \left(\frac{1}{t - t_r} \int_0^{t-t_r} \tau \mu_{mm}(\tau) d\tau \right) \\ &\equiv \alpha_m a_m(t) + \beta_m a_m(t_r) \quad \text{for } t_r < t \leq t_{r+1}. \end{aligned} \quad (30a)$$

Clearly,

$$\int_0^{t-t_r} \mu_{mm}(\tau) a_m(t - \tau) d\tau = 0 \quad \text{when } t = t_r. \quad (30b)$$

In the above equations we have set

$$\alpha_m = \int_0^{t-t_r} \mu_{mm}(\tau) d\tau - \frac{1}{t - t_r} \int_0^{t-t_r} \tau \mu_{mm}(\tau) d\tau$$

and

$$\beta_m = \frac{1}{t - t_r} \int_0^{t-t_r} \tau \mu_{mm}(\tau) d\tau.$$

It follows from equations (27)–(30) that for $t_r < t \leq t_{r+1}$

$$\sum_{n=1}^N \int_0^t \mu_{mn}(\tau) a_n(t - \tau) d\tau = \alpha_m a_m(t) + \beta_m a_m(t_r) + \sum_{n=1}^N \int_{t-t_r}^t \mu_{mn}(\tau) a_n(t - \tau) d\tau \quad (31a)$$

and when $t = t_r$

$$\sum_{n=1}^N \int_0^{t_r} \mu_{mn}(\tau) a_n(t_r - \tau) d\tau = \sum_{n=1}^N \int_0^{t_r} \mu_{mn}(\tau) a_n(t_r - \tau) d\tau. \quad (31b)$$

The only acceleration on the right-hand-side of equation (31) that corresponds to a time greater than t_r is the term containing $a_m(t)$. We will combine this term with the $a_m(t)$ term on the left-hand-side of equation (21a). Combining equation (31) with equation (21a), we get

$$(M + \alpha_m) a_m(t) + R v_m(t) + K u_m(t) = F(t) - \beta_m a_m(t_r) - \sum_{n=1}^N \int_{t-t_r}^t \mu_{mn}(\tau) a_n(t - \tau) d\tau \quad \text{for } t_r < t \leq t_{r+1} \quad (32a)$$

and

$$M a_m(t_r) + R v_m(t_r) + K u_m(t_r) = F(t_r) - \sum_{n=1}^N \int_0^{t_r} \mu_{mn}(\tau) a_n(t_r - \tau) d\tau. \quad (32b)$$

The right-hand-side of equation (32) contains only known accelerations at times up through t_r . Solving equation (32) for a_m , we get

$$a_m(t) = \frac{1}{M + \alpha_m} \left[F_m(t) - Rv_m(t) - Ku_m(t) - \beta_m a_m(t_r) - \sum_{n=1}^N \int_{t-t_r}^t \mu_{mn}(\tau) a_n(t - \tau) d\tau \right] \quad t_r < t \leq t_{r+1} \quad (33a)$$

and

$$a_m(t_r) = \frac{1}{M} \left[F_m(t_r) - Rv_m(t_r) - Ku_m(t_r) - \sum_{n=1}^N \int_0^{t_r} \mu_{mn}(\tau) a_n(t_r - \tau) d\tau \right]. \quad (33b)$$

Combining equation (33) with the equations in (21), we get

$$\dot{v}_m(t) = \frac{1}{M + \alpha_m} \left[F_m(t) - Rv_m(t) - Ku_m(t) - \beta_m a_m(t_r) - \sum_{n=1}^N \int_{t-t_r}^t \mu_{mn}(\tau) a_n(t - \tau) d\tau \right] \quad (34a)$$

$$\dot{u}_m(t) = v_m(t) \quad \text{for } t_r < t \leq t_{r+1} \quad (34b)$$

and

$$\dot{v}_m(t_r) = \frac{1}{M} \left[F_m(t_r) - Rv_m(t_r) - Ku_m(t_r) - \sum_{n=1}^N \int_0^{t_r} \mu_{mn}(\tau) a_n(t_r - \tau) d\tau \right] \quad (34c)$$

$$\dot{u}_m(t_r) = v_m(t_r). \quad (34d)$$

In addition, the functions $u_m(t)$ and $v_m(t)$ are known at the initial time t_r of the interval. Therefore, the above pair of equations along with the initial conditions at t_r comprise a standard system of first order ordinary differential equations of the form

$$\begin{aligned} \dot{y}(t) &= f(y(t), t) \\ y(t_0) &= y_0 \end{aligned} \quad (35)$$

where y is a vector-valued function of time. If there had been nonlinearities in equation (21) that didn't involve the acceleration a_m , these would have ended up on the right-hand-side of equation (35). Any standard differential equation solver can be used to advance the solution to the next time step. Notice that our assumption on the size of the time step has allowed us to partially decouple the array problem. The coupling between elements is contained entirely in the known histories of the accelerations. At each time step the system of differential equations (34) is solved to advance the solution to the next time step. This is done separately for each element in the array. The history of each a_n is then updated using equation (33) in preparation for the next time step.

The results that will be presented for our example problems were computed using a second-order Runge-Kutta method known as Heun's method. This method advances the solution to the system of differential equations (35) from t_r to t_{r+1} using

$$y(t_{r+1}) = y(t_r) + \frac{1}{2}\delta[\dot{y}(t_r) + f(y(t_r) + \dot{y}(t_r)\delta, t_{r+1})]. \quad (36)$$

Here $\dot{y}(t_r) = f(y(t_r), t_r)$. Although this is a fairly crude method, it has the advantage of only involving quantities evaluated at the times t_r and t_{r+1} . In our example problems, y and f can be written in terms of components as follows:

$$y = \begin{pmatrix} y_1 \\ y_2 \end{pmatrix} \quad \text{and} \quad f(y, t) = \begin{pmatrix} f_1(y, t) \\ f_2(y, t) \end{pmatrix}. \quad (37)$$

Referring to equation (34), we see that

$$f_1(y, t) = \frac{1}{M + \alpha_m} \left[F_m(t) - Ry_1 - Ky_2 - \beta_m a_m(t_r) - \sum_{n=1}^N \int_{t-t_r}^t \mu_{mn}(\tau) a_n(t - \tau) d\tau \right] \quad (38a)$$

$$f_2(y, t) = y_1 \quad \text{for } t_r < t \leq t_{r+1} \quad (38b)$$

and

$$f_1(y, t_r) = \frac{1}{M} \left[F_m(t_r) - Ry_1 - Ky_2 - \sum_{n=1}^N \int_0^{t_r} \mu_{mn}(\tau) a_n(t_r - \tau) d\tau \right] \quad (38c)$$

$$f_2(y, t_r) = y_1. \quad (38d)$$

To apply Heun's method to the example problems, we need to evaluate $f(y, t)$ at the times t_r and t_{r+1} . Equations (38c) and (38d) provide the value of $f(y, t)$ at t_r . It follows from equations (38a) and (38b) that

$$f_1(y, t_{r+1}) = \frac{1}{M + \alpha_m} \left[F_m(t_{r+1}) - Ry_1 - Ky_2 - \beta_m a_m(t_r) - \sum_{n=1}^N \int_{\delta}^{t_{r+1}} \mu_{mn}(\tau) a_n(t_{r+1} - \tau) d\tau \right] \quad (39a)$$

$$f_2(y, t_{r+1}) = y_1. \quad (39b)$$

We will now look at the approximation of the integrals occurring in equations (38c) and (39a). Clearly,

$$\int_0^{t_r} \mu_{mn}(\tau) a_n(t_r - \tau) d\tau = \sum_{k=0}^{r-1} \int_{t_k}^{t_{k+1}} \mu_{mn}(\tau) a_n(t_r - \tau) d\tau \quad (40)$$

$$\int_{\delta}^{t_{r+1}} \mu_{mn}(\tau) a_n(t_{r+1} - \tau) d\tau = \sum_{k=1}^r \int_{t_k}^{t_{k+1}} \mu_{mn}(\tau) a_n(t_{r+1} - \tau) d\tau. \quad (41)$$

Since μ_{mn} typically varies faster than a_n , we will approximate the integrals by assuming that a_n varies linearly over each interval $[t_k, t_{k+1}]$, i.e.,

$$a_n(t_r - \tau) = \frac{a_n(t_{r-k-1}) - a_n(t_{r-k})}{\delta} \tau + \frac{t_{k+1} a_n(t_{r-k}) - t_k a_n(t_{r-k-1})}{\delta} \quad (42)$$

for $t_k \leq \tau \leq t_{k+1}$.

Using this relation, it follows that

$$\begin{aligned} \int_{t_k}^{t_{k+1}} \mu_{mn}(\tau) a_n(t_r - \tau) d\tau &\doteq a_n(t_{r-k}) \left[\frac{t_{k+1}}{\delta} \int_{t_k}^{t_{k+1}} \mu_{mn}(\tau) d\tau - \frac{1}{\delta} \int_{t_k}^{t_{k+1}} \tau \mu_{mn}(\tau) d\tau \right] \\ &+ a_n(t_{r-k-1}) \left[\frac{1}{\delta} \int_{t_k}^{t_{k+1}} \tau \mu_{mn}(\tau) d\tau - \frac{t_k}{\delta} \int_{t_k}^{t_{k+1}} \mu_{mn}(\tau) d\tau \right]. \end{aligned} \quad (43)$$

The integrals on the right-hand-side of equation (43) can be approximated using the trapezoidal rule. Replacing r with $r + 1$ in equation (43), we obtain

$$\begin{aligned}
\int_{t_k}^{t_{k+1}} \mu_{mn}(\tau) a_n(t_{r+1} - \tau) d\tau \doteq & a_n(t_{r+1-k}) \left[\frac{t_{k+1}}{\delta} \int_{t_k}^{t_{k+1}} \mu_{mn}(\tau) d\tau \right. \\
& \left. - \frac{1}{\delta} \int_{t_k}^{t_{k+1}} \tau \mu_{mn}(\tau) d\tau \right] \\
& + a_n(t_{r-k}) \left[\frac{1}{\delta} \int_{t_k}^{t_{k+1}} \tau \mu_{mn}(\tau) d\tau \right. \\
& \left. - \frac{t_k}{\delta} \int_{t_k}^{t_{k+1}} \mu_{mn}(\tau) d\tau \right].
\end{aligned} \tag{44}$$

The integrals on the right-hand-sides of equations (43) and (44) can be computed up to the time where they become negligible prior to starting the time stepping.

7 Computed Results for Some Transducer Arrays

In this section we will present some computed results based on the techniques developed in the previous sections. The frequency domain acoustic calculations were performed using the CHIEF and AXICHIEF programs[2, 3]. The remainder of the calculations were performed using Matlab. All of the computations were done on a standard PC. We chose example problems that are linear, since this allows us to check the results in the time domain by solving the array problem in the frequency domain for a large range of frequencies and then using the inverse Fourier transform to calculate the element accelerations in the time domain. Except where noted all examples will have zero internal losses. We will first consider a single element. The first two figures show the transient behavior of the acceleration when the element forcing function consists of a pulse that is one half cycle of a sine wave. For figure 11 the parameters were chosen to make $s/\lambda_m = 0.2$, and the frequency of the drive pulse was chosen to make $s/\lambda = 0.22$. For figure 12 the parameters were chosen to make $s/\lambda_m = 0.1$, and the frequency of the drive pulse was chosen to make $s/\lambda = 0.11$. The agreement between the results calculated in the time domain and those calculated by transforming frequency domain results is quite good. Notice that the second case rings longer since the radiation loss at the lower resonant frequency is less.

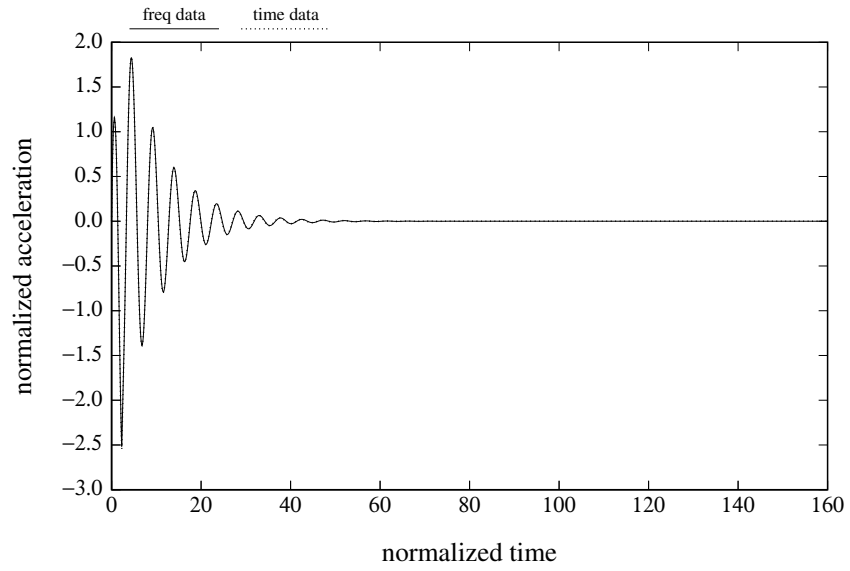


Figure 11: Acceleration of pulsed single element ($s = 0.22\lambda$).

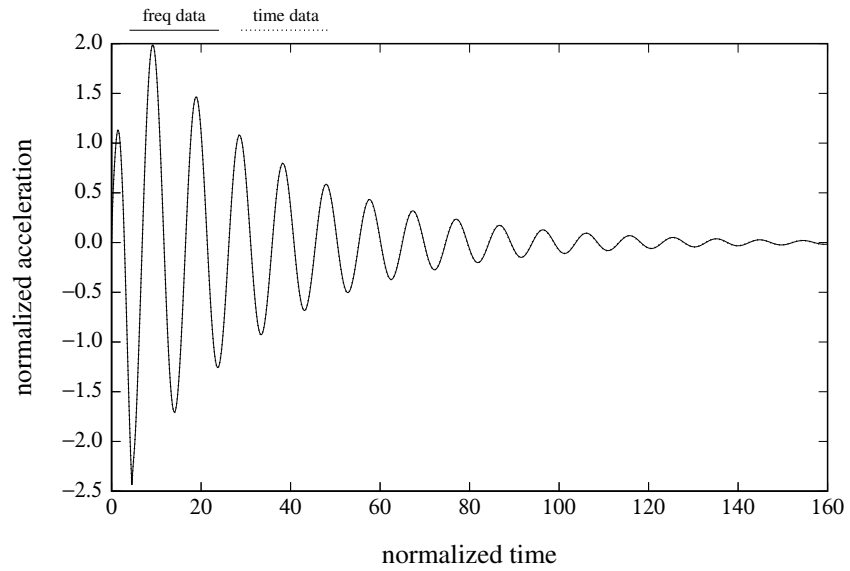


Figure 12: Acceleration of pulsed single element ($s = 0.11\lambda$).

Figure 13 shows the acceleration for a sinusoidal drive with frequency corresponding to $s/\lambda = 0.11$. The parameters were chosen so as to make $s/\lambda_m = 0.1$. Notice that the response has a transient period and then settles in to a steady state. The steady state amplitude and phase were calculated by fitting a function of the form $A \sin [2\pi(s/\lambda)t + \phi]$ to the tail end of the response in a least-squares sense. For this case the computed amplitude was 11.1 and the phase was 43.8 degrees. The steady state amplitude and phase calculated in the frequency domain for this frequency were 11.0 and 43.4 degrees respectively. This amounts to only a 0.9% difference in amplitude and a 0.4 degree difference in phase.

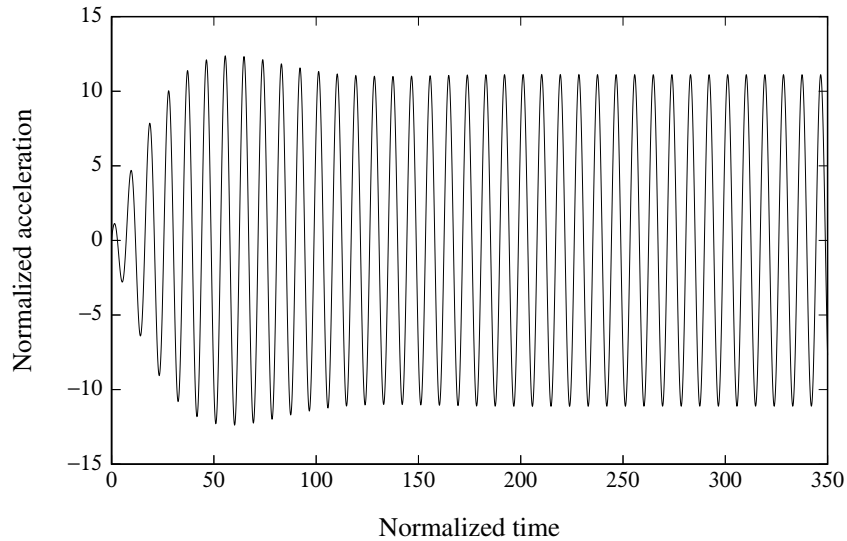


Figure 13: Sinusoidal drive of single element ($s = 0.11\lambda$).

Figures 14 and 15 show a comparison of the steady-state amplitude and phase calculated in the time domain and the frequency domain for a range of frequencies. Again the agreement is quite good.

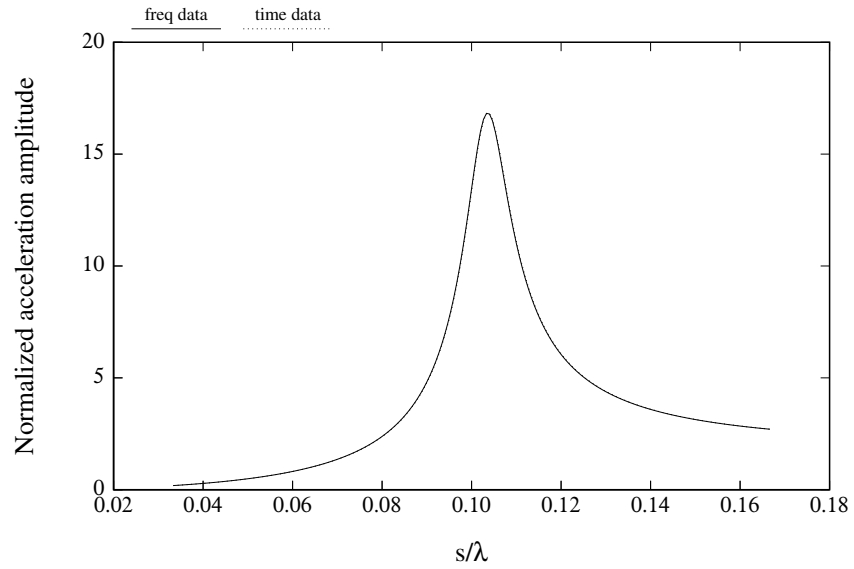


Figure 14: Steady state amplitude vs. frequency for single element.

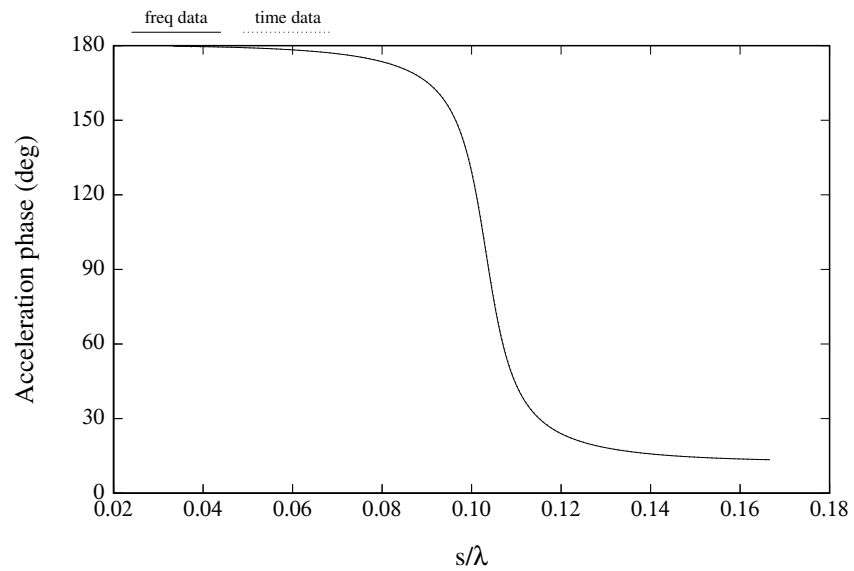


Figure 15: Steady state phase vs. frequency for single element.

We will now look at some array results. The first two array examples correspond to a half cycle pulse forcing function with $s/\lambda = 0.22$ and an array spacing of $d = 2s$. The parameters were chosen so as to make $s/\lambda_m = 0.2$. Figure 16 shows the acceleration of the center element of a three element array and figure 17 shows the acceleration of the center element of a five element array. Notice that the agreement between the time-domain results and those calculated by transforming the frequency-domain results is quite good.

Figures 18–21 show similar results for three, four, five and six element arrays when $s/\lambda = 0.11$ and $s/\lambda_m = 0.1$. Notice that the agreement between the time-domain results and those calculated by transforming the frequency-domain results is quite good except for the five element array. It turns out that the radiation loading for the five element array was an order of magnitude smaller than for the other arrays. Thus the frequency response for the five element array has a much sharper resonance than the other cases and is more sensitive to small changes. This may be responsible for the poorer agreement in this case. Notice also that the decay is much slower for the cases with $s/\lambda_m = 0.1$ than it was for the cases with $s/\lambda_m = 0.2$. The cases with $s/\lambda_m = 0.1$ correspond to a much stronger array interaction environment since the elements are small in wavelength and closely spaced in wavelength near resonance. In addition the element internal response at resonance provides no help in controlling the array accelerations. In fact some of the elements are taking in power rather than radiating power.

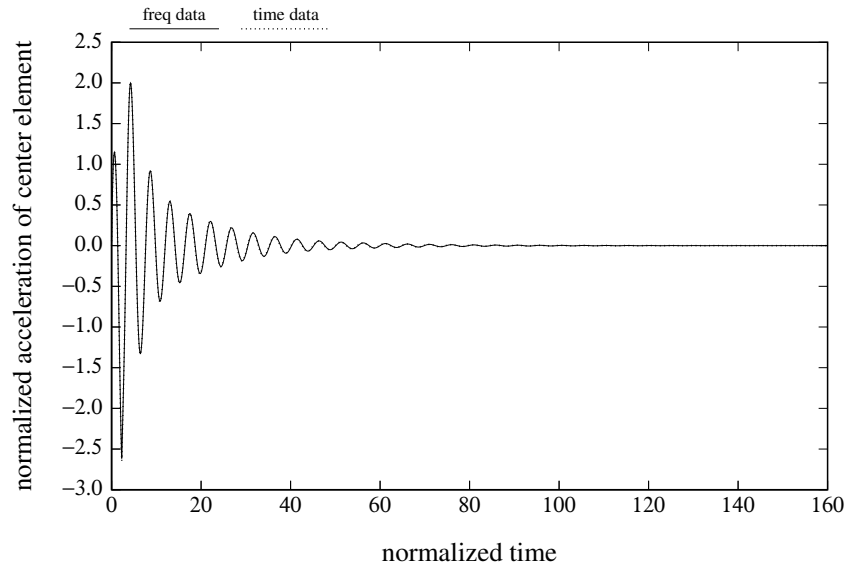


Figure 16: Center element of pulsed 3 element array ($s = 0.22\lambda$).

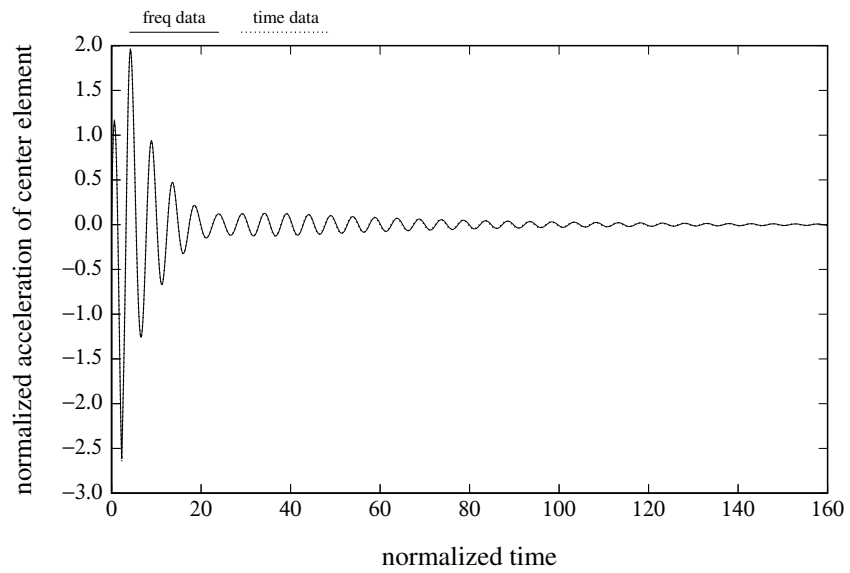


Figure 17: Center element of pulsed 5 element array ($s = 0.22\lambda$).

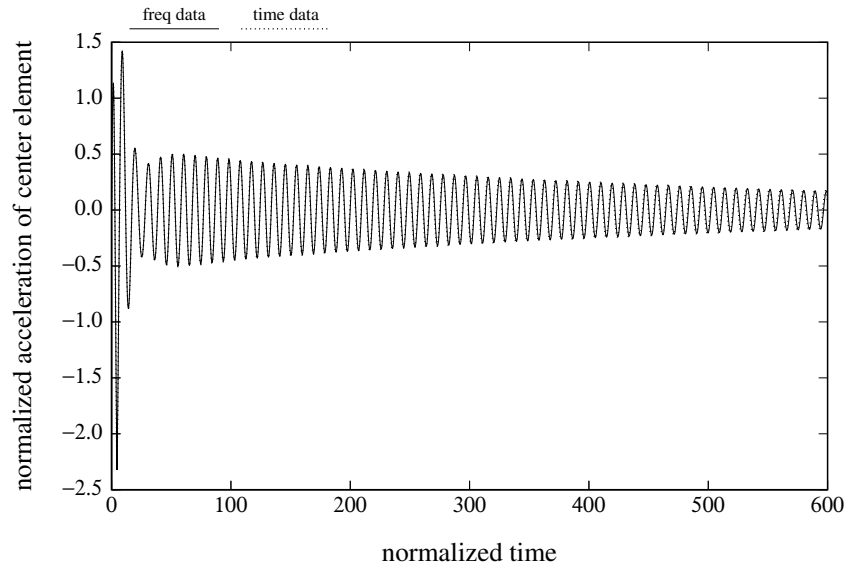


Figure 18: Center element of pulsed 3 element array ($s = 0.11\lambda$).

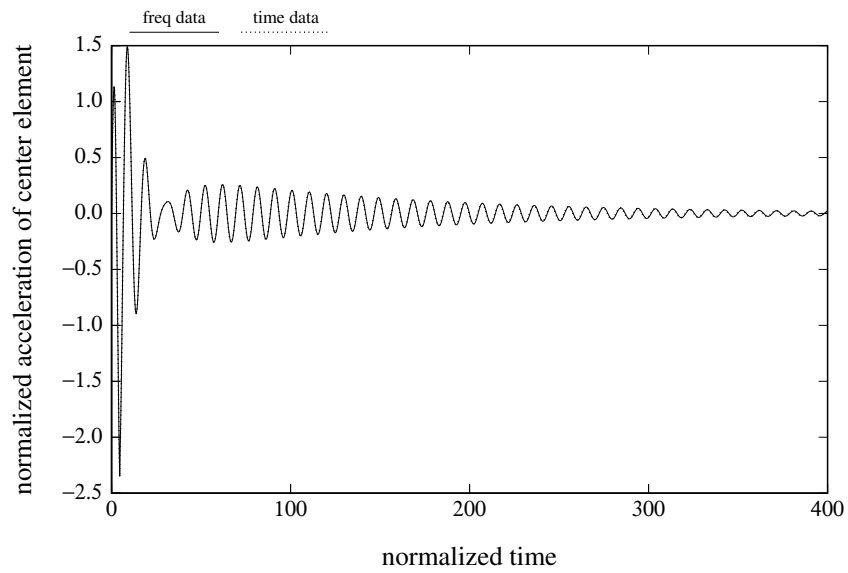


Figure 19: Center element of pulsed 4 element array ($s = 0.11\lambda$).

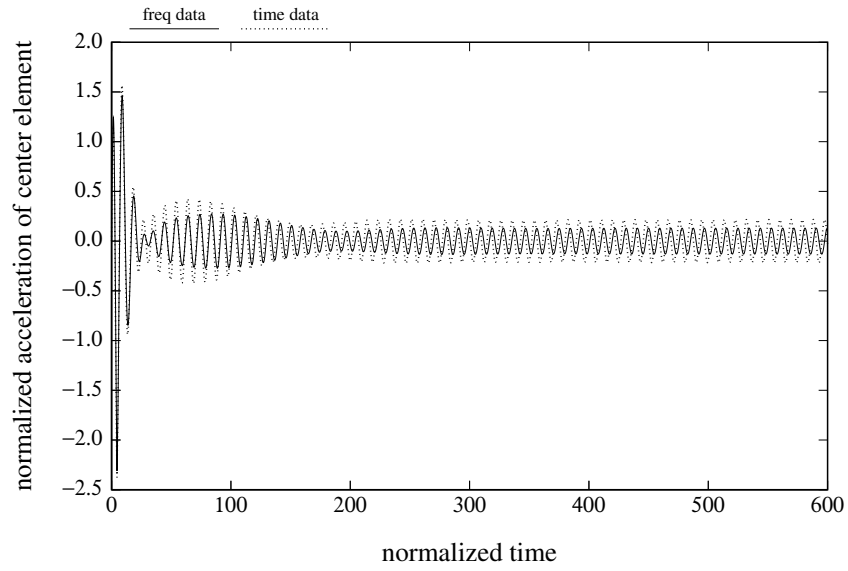


Figure 20: Center element of pulsed 5 element array ($s = 0.11\lambda$).

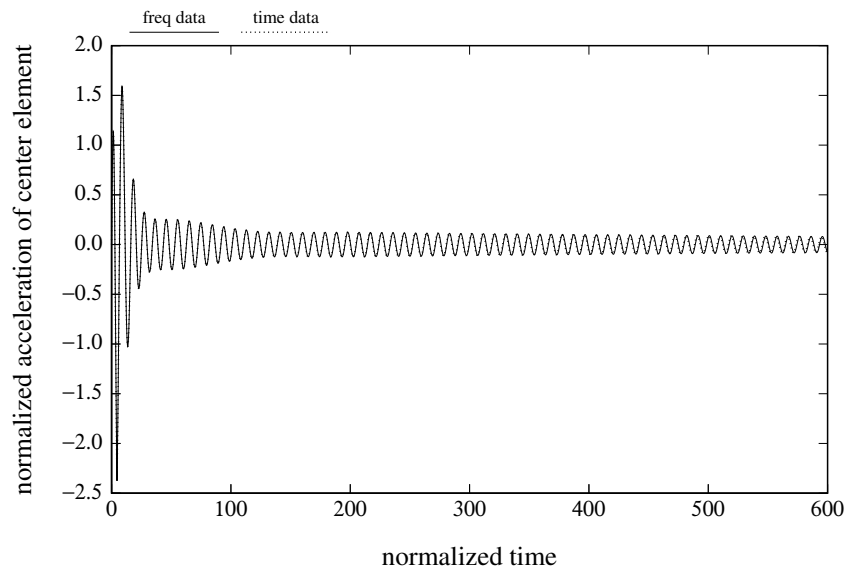


Figure 21: Center element of pulsed 6 element array ($s = 0.11\lambda$).

We will now look at the effect of internal losses. Figure 22 shows the five element case when the internal loss is set so as to make $Q = 100$. Figure 23 shows the five element case when the internal loss is set so as to make $Q = 20$. In these cases the agreement between the time-domain results and those calculated by transforming the frequency-domain results is quite good. As we would suspect, the decay is faster when the internal losses are greater.

Figures 24 and 25 show the acceleration response to a sinusoidal drive for the center element of a three element array and a four element array when $s/\lambda_m = 0.1$, $s/\lambda = 0.11$. The steady state response of the center element of the three element array computed from the time response had an amplitude of 5.393 and a phase of 102 degrees. The corresponding result computed in the frequency domain had an amplitude of 5.387 and a phase of 100.6 degrees. Thus, there is only a 0.1% difference in amplitude and a 1.4 degree difference in phase. The steady state response of one of the center elements of the four element array computed from the time response had an amplitude of 6.338 and a phase of 85.4 degrees. The corresponding result computed in the frequency domain had an amplitude of 6.341 and a phase of 84.9 degrees. In this case there was only a 0.05% difference in amplitude and a 0.5 degree difference in phase. It should be noted that the time to reach steady state is surprisingly long for these closely packed arrays of elements that are small in wavelength. The period of the sinusoidal forcing function in scaled time is $1/0.11 = 9.091$. Thus it takes on the order of 150–200 cycles for the center element of the three element array to reach steady state or about 300 times longer than it takes a sound wave to cross the array.

Figures 26 and 27 show the effect of internal losses on the time to reach steady state. Notice that the transient time becomes progressively shorter as Q decreases (losses become greater).

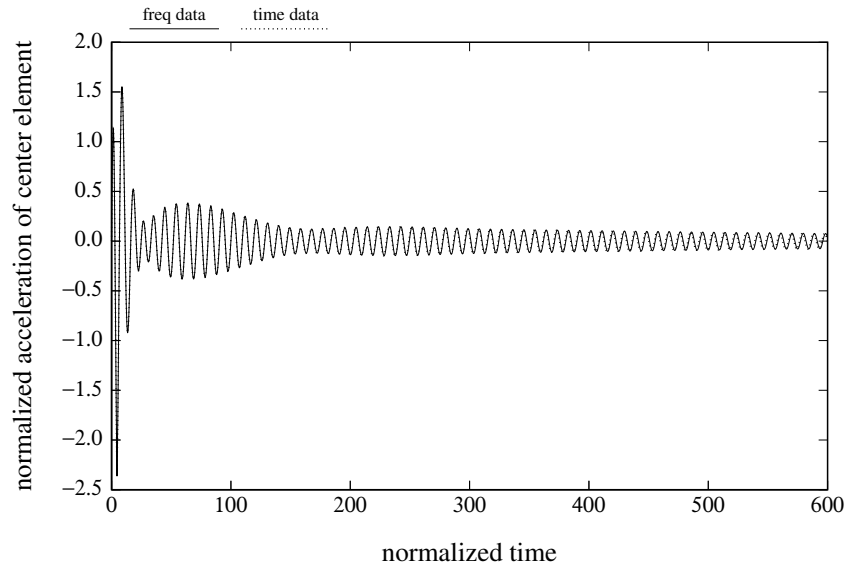


Figure 22: Center element of pulsed 5 element array with $Q=100$ ($s = 0.11\lambda$).

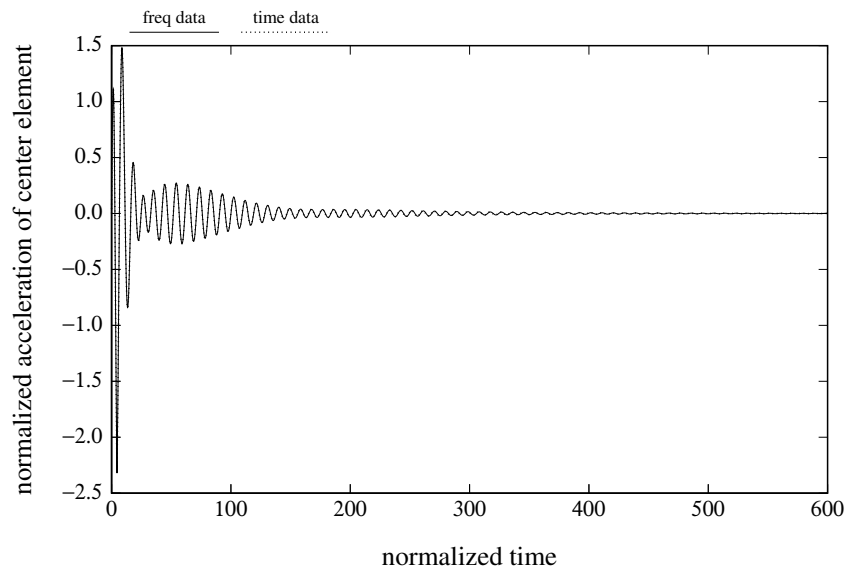


Figure 23: Center element of pulsed 5 element array with $Q=20$ ($s = 0.11\lambda$).

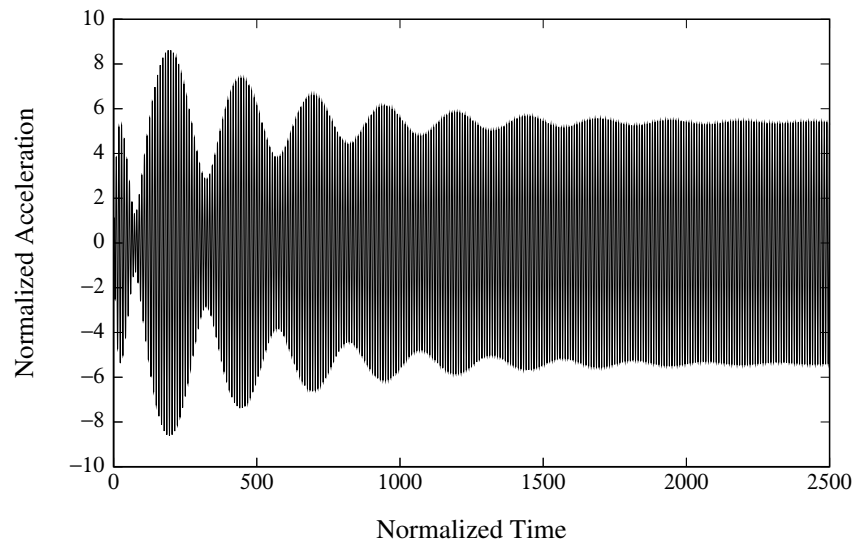


Figure 24: Center element of 3 element array with sinusoidal drive ($s = 0.11\lambda$).

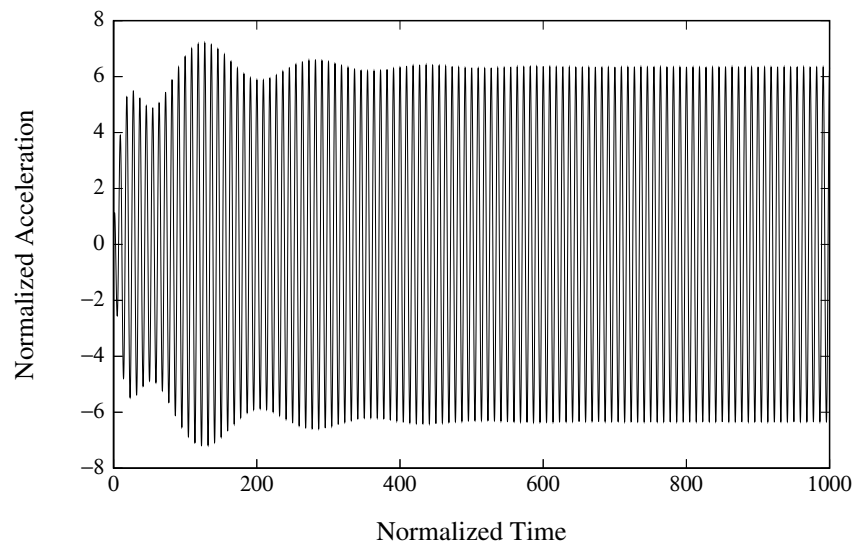


Figure 25: Center element of 4 element array with sinusoidal drive ($s = 0.11\lambda$).

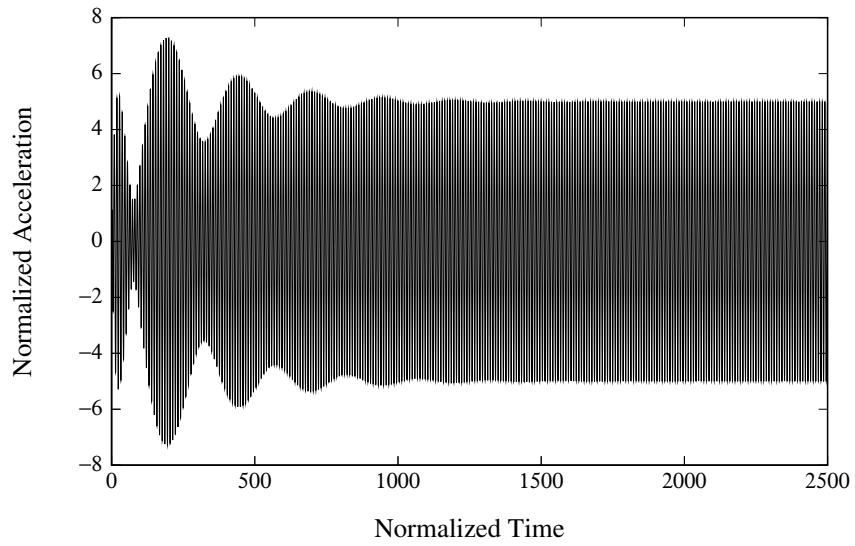


Figure 26: Center element of 3 element array with sinusoidal drive ($s = 0.11\lambda$ and $Q = 100$).

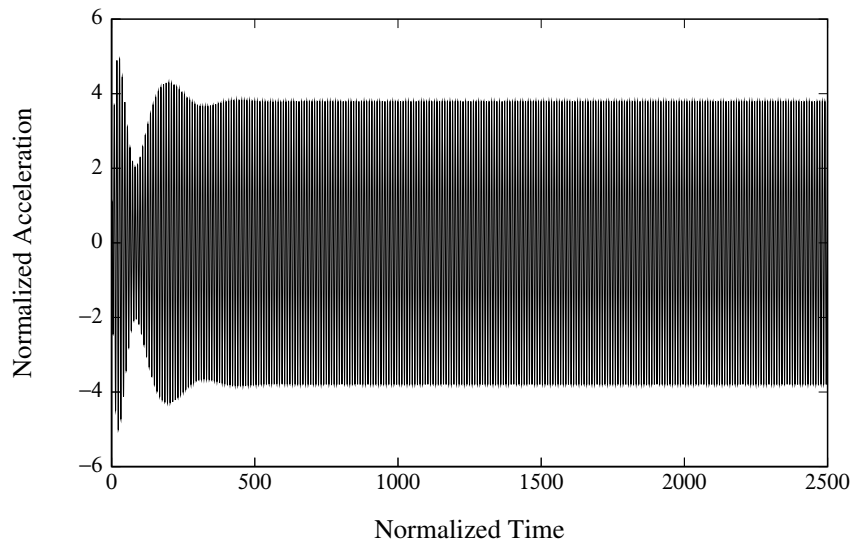


Figure 27: Center element of 3 element array with sinusoidal drive ($s = 0.11\lambda$ and $Q = 20$).

8 Summary

In this paper we have described a technique for computing acoustic array interactions in the time domain. This technique makes use of mutual radiation impulse functions. These impulse functions are calculated in the frequency domain using the CHIEF or AXICHIEF program and then converted to the time domain by means of the inverse Fourier transform. A special technique was developed involving modified impulse response functions that improved the convergence rate in the frequency domain from $1/\omega$ to $1/\omega^3$. This greatly improved the small time accuracy of the radiation impulse functions and reduced the range of frequencies that needed to be calculated. Although the techniques developed in this paper can be used for arrays of nonlinear elements as well as for arrays of linear elements, the computed results in this paper are for linear elements since it is much easier to provide checks of the accuracy using frequency domain techniques. In general the comparison of results computed in the time domain with those obtained by transforming frequency domain results was quite good. However, there was one case (five element array with element size and spacing small in wavelength) where the comparison was not as good. It turns out that this case had a very sharp resonance response due to very small acoustic loading. For arrays driven with sinusoidal forcing functions the time to reach steady state was surprisingly long for the cases where the frequency was near resonance, there were no losses, and the element size and spacing were small compared to the wavelength at resonance.

As far as possible extensions of this work, it would be interesting to apply the techniques used here to arrays in which the transducers are multimode devices or have nonlinearities. It also seems likely that direct methods employing the Kirchhoff integral equation would also benefit from replacing the pressure due to an impulse by a modified pressure that didn't have discontinuities at time zero.

References

- [1] Benthien,G., *Calculation of Acoustic Loading on Transducers in the Time Domain*, Proceedings of OCEANS 2003 Conference, Session 110, 2079–2082 (2003)
- [2] Benthien,G., Barach,D., and Hobbs,S., CHIEF 2004 Users Manual, Technical Document 3180, SPAWAR Systems Center, San Diego, April 2004
- [3] Benthien,G. and Hobbs, S., AXICHIEF 2004 Users Manual, Unpublished Technical Document, SPAWAR Systems Center, San Diego
- [4] Lindemann, O., *Transient fluid reaction on a baffled plane piston of arbitrary shape*, J. Acoust. Soc. Am., vol.55, No. 4, April 1974